

Lanthanide-based nanostructures for optical bioimaging: Small particles with large promise

Eva Hemmer, Fiorenzo Vetrone, and Kohei Soga

Fast and significant progress has been achieved in the development of new biomarkers in recent years providing promising approaches for the reliable detection of diseases at an early stage. Yet, the disadvantages of commonly used markers, including photobleaching, autofluorescence, phototoxicity, and scattering, when ultraviolet or visible light is used for excitation, need to be overcome. Lanthanide-doped host materials are well known for their excellent optical properties, such as their ability to (up)convert near-infrared excitation to higher energies spanning the ultraviolet, visible, and near-infrared regions or to undergo strong near-infrared luminescence following near-infrared excitation. Their application as biomarkers may overcome the aforementioned drawbacks of conventional dyes. Thus, lanthanide-based nanostructures are highly promising candidates for cellular and small animal imaging, while the assessment of their cytotoxicity remains a crucial issue. Recent developments in the field of upconversion and near-infrared bioimaging focusing on some of the latest results obtained in *in vitro* and *in vivo* studies assessing the toxicity of lanthanide-based nanophosphors are highlighted in this review.

Taking advantage of near-infrared light and upconversion

Bioimaging plays a crucial role in medicine, where reliable and fast diagnosis of diseases at an early stage is essential for successful treatment. In optical bioimaging, fluorescent proteins or organic dyes are the most common markers. Yet, these conventional fluorescent markers suffer from color fading restricting their temporal use, autofluorescence of the biological tissue (leading to background emission overlaying the emission of interest from the marker, thus resulting in reduced image contrast), phototoxicity, and scattering when ultraviolet (UV) light is used as the excitation source. Much effort has been undertaken to overcome these limitations. The use of near-infrared (NIR) light brings several advantages, such as reduced scattering by biological tissue and consequently deeper penetration depth when the wavelengths are located within the biological window (**Figure 1**).[1,2]

Of particular interest for *in vivo* imaging is the wavelength region over 1000 nm providing penetration depths in the range of several centimeters in comparison to only a few micrometers to millimeters when UV or visible (VIS) light is used. Consequently, NIR fluorescent markers are attracting increasing attention and are being investigated in preclinical studies or are already successfully applied in biolabeling or as an image-guidance tool for surgery.[4]

The class of lanthanide-based compounds is still underrepresented in such preclinical studies, yet interest in lanthanide-based biomarkers for NIR bioimaging is rapidly expanding due to their outstanding optical and magnetic properties.[5] These are due to the electron configuration of the trivalent lanthanide ions (Ln^{3+}), which are characterized by an incompletely filled $4f$ shell that is located inside the complete $5s^2$ and $5p^6$ shells, resulting in shielding of the $4f$ electrons from the local microenvironment.[6–8] Consequently, Ln^{3+} ions doped into a suitable host exhibit narrow optical absorption and emission bands, high emission efficiency, and long excited state lifetimes. Further, the different electronic configurations of each Ln^{3+} ion result in different emission wavelengths, allowing multicolor applications.

So-called upconversion emission is of particular interest for NIR-bioimaging. This phenomenon is well-known for Ln^{3+} ions, such as Er^{3+}, doped into a suitable host material

Eva Hemmer, Institut National de la Recherche Scientifique, Centre Énergie Matériaux Télécommunication, Université du Québec, Canada; eva.hemmer@emt.inrs.ca
Fiorenzo Vetrone, Institut National de la Recherche Scientifique, Centre Énergie Matériaux Télécommunication, Université du Québec, Canada; vetrone@emt.inrs.ca
Kohei Soga, Department of Materials Science and Technology, Tokyo University of Science, Japan; mail@ksoga.com
DOI: 10.1557/mrs.2014.223

© 2014 Materials Research Society
https://doi.org/10.1557/mrs.2014.223 Published online by Cambridge University Press

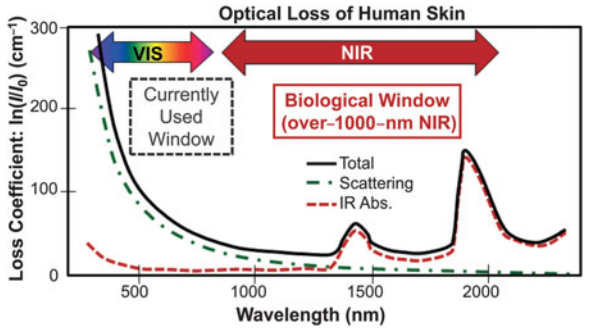


Figure 1. Absorption spectrum of human skin showing the biological window. The reduced total absorption by biological tissue such as human skin of near-infrared (NIR) light when compared to visible light allows for deeper penetration depth into biological samples, which makes the use of NIR light of high interest for biomedical applications. Adapted with permission from Reference 3. © 2013 The Royal Society of Chemistry. Note: VIS, visible; I_0, flux of incident beam; I, flux over a layer of human skin of a specific thickness.[1]

(e.g., Y_2O_3 or Gd_2O_3) absorbing in the NIR range (980 nm) and emitting green (550 nm) and red (670 nm) light (**Figure 2**a). Here, NIR light of lower energy is used for the stepwise excitation, followed by the emission of higher energy light (Figure 2b).[7,10,11] Co-doping with Yb^{3+} ions is applied for sensitizing and enhancing the emission intensity. Further, the emission of NIR light under NIR excitation is known for Ln^{3+}-doped host materials (Figure 2c). The excited Yb^{3+} ions transfer their energy to the Er^{3+} ions, resulting in their excitation. Subsequent decay to the ground level leads to the emission of 1.5 μm light (Figure 2d).

Facing the need for fast and reliable medical diagnosis, there is a push for the development of new biomarkers that overcome the drawbacks of those commonly used and whose excitation and emission wavelengths are ideally within the range of the biological window. Aside from the optical requirements, important concerns about their toxicity need to be addressed, and the toxicity assessment is a crucial step toward new optical biomarkers.

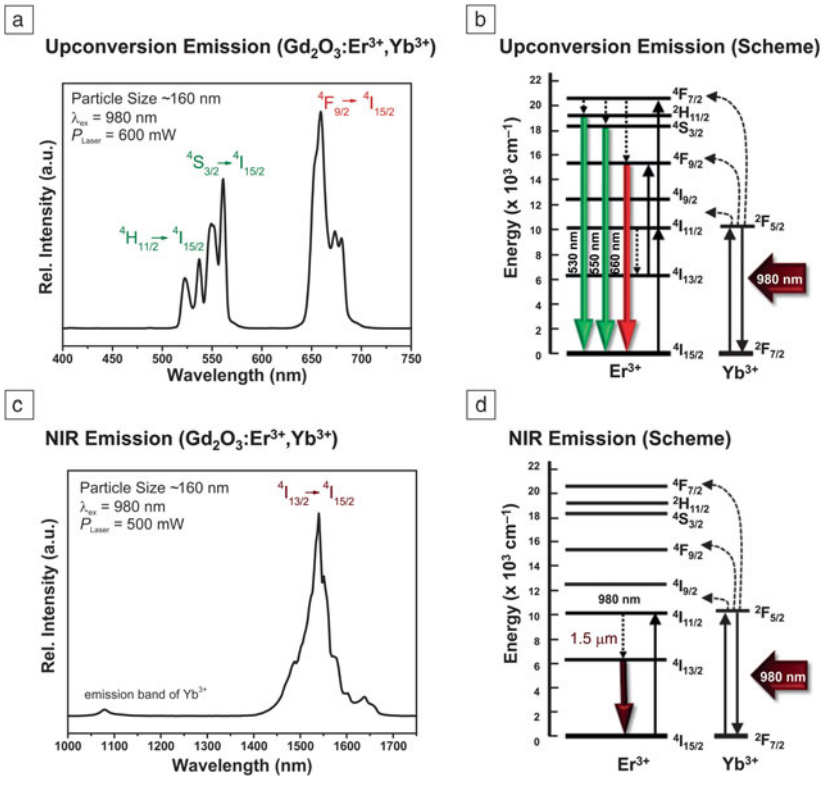


Figure 2. Duality of Ln^{3+}-doped host materials emitting both visible (upconversion emission) and near-infrared (NIR) light under NIR excitation. (a) and (c) show photoluminescence spectra recorded on Gd_2O_3:Er^{3+},Yb^{3+} nanoparticles under 980 nm excitation exhibiting the characteristic emission peaks in the visible and NIR range. Those peaks can be assigned to the transitions between energy levels of Er^{3+}- and Yb^{3+}-ions upon 980 nm excitation as illustrated in schemes (b) and (d) (green and red arrows symbolize the emission of green and red light, respectively; the dark red arrow symbolizes the emission of NIR light). (a and c) Reproduced with permission from Reference 9. © 2012 Springer. (b and d) Reproduced with permission from Reference 3. © 2013 The Royal Society of Chemistry. Note: The transitions in the figure are expressed by $^{2S+1}L_J$ (S, total spin quantum number; J, total angular momentum quantum number; L, total orbital angular momentum quantum number) expression for the 4*f* energy levels of rare-earth ions; λ_{ex}, excitation wavelength; P_{Laser}, power of the laser used for excitation.

Cytotoxicity assessment of lanthanide-based nanophosphors

Lanthanide oxide nanoparticles

Yttrium oxide is well-known for its photodurability and low phonon energy, which makes Ln^{3+}-doped Y_2O_3 nanoparticles (Y_2O_3: Ln^{3+}) very attractive for optical applications, including bioimaging.[12,13] However, prior to their application in biomedicine, any potential toxicity of these nanoparticles must be ruled out; three aspects are mainly addressed in the literature: (1) dosage, (2) surface modification, and (3) size and morphology. During the last decade, several studies have investigated upconverting and NIR-emitting nanophosphors with regard to these aspects.

For instance, concentration-dependent *in vitro* cytotoxicity studies on Y_2O_3:Er^{3+} nanoparticles revealed their uptake by macrophages (cells that consume foreign material), thus inducing increased cell death with increasing dosage (**Figure 3**a).[14] For the same nanoparticles, no cytotoxic effect was found toward non-phagocytic B-cell hybridomas, which are fused hybrid cells—between B-cells (a type of lymphocyte) and myeloma tumor cells—that do not uptake foreign material. The cytotoxic effect toward macrophages was ascribed to the poor chemical stability of Y_2O_3 under acidic conditions, as found inside these cells. Consequently, careful surface modification of the nanophosphors providing chemical stability (as well as dispersion stability in biological fluids, biocompatibility, site-selectivity [toward cancerous cells], and controlled clearance from

https://doi.org/10.1557/mrs.2014.223 Published online by Cambridge University Press

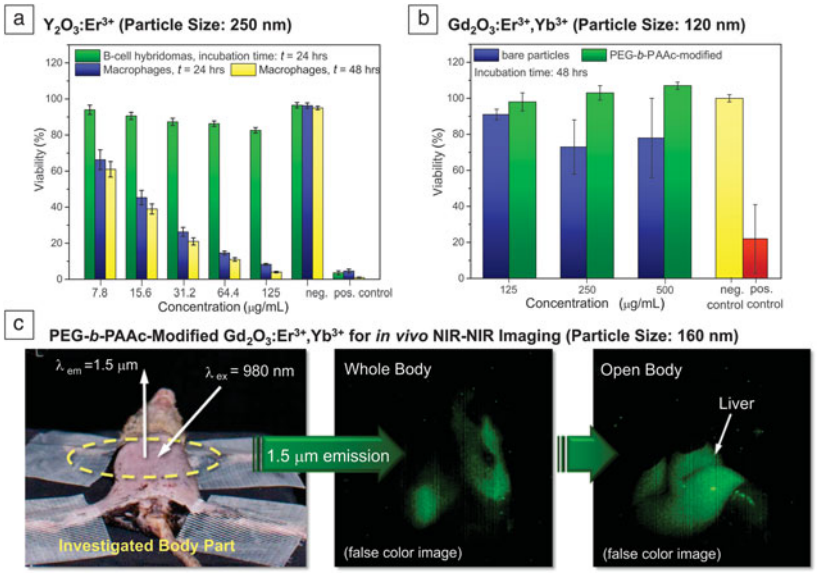


Figure 3. (a) Cytotoxic behavior of $Y_2O_3:Er^{3+}$. The uptake of the nanoparticles by macrophages results in the decrease of their viability with increasing particle concentration due to the toxic effect of Y^{3+}-ions leaking from the particles once uptaken by the macrophages. In contrast, no significant reduction in viability is observed for B-cell hybridomas, which generally show less or no tendency to uptake foreign material. (b) Cytotoxic behavior of $Gd_2O_3:Er^{3+},Yb^{3+}$. The surface modification with PEG-*b*-PAAc results in increased viability when compared to bare nanostructures, which is ascribed to an improved chemical stability and therefore reduced formation of toxic Gd^{3+}-ions upon uptake by the macrophages. (c) Over-1000 nm fluorescence bioimaging of a mouse. White arrows represent the 980 nm laser light used for excitation as well as the emitted near-infrared (NIR) light of 1.5 μm wavelength. The emission of 1.5 μm light can be seen through the skin of the mouse, revealing the high potential of NIR light for deep-tissue *in vivo* imaging. The bright 1.5 μm emission mainly originates from particles accumulated in the liver, as obvious from images taken of the opened mouse body (size of the liver in the range of 1 to 2 cm). (a) Reproduced with permission from Reference 3. © 2013 The Royal Society of Chemistry. (b) Adapted with permission from Reference 27. © 2013 Elsevier. (c) Reproduced with permission from Reference 9. © 2012 Springer. Note: PEG-*b*-PAAc, poly(ethylene glycol)-*b*-poly(acrylic acid) block co-polymer; λ_{ex}, excitation wavelength; λ_{em}, emission wavelength; *t*, incubation time; negative control: incubation in cell culture medium without nanostructures; positive control: anticancer drug carboplatin (100 μg mL^{-1}).

the organism) is a general and essential requirement. Herein, SiO_2 and polymer-based coatings are suitable to prevent cytotoxicity and unspecific interference with cells, improving the *in vivo* biodistribution.[15–18] It was further shown that the functionalization of $Y_2O_3:Er^{3+},Yb^{3+}$ with amine groups allows specific surface immobilization, and provides water-dispersibility, biocompatibility, and the ability for bioconjugation.[19]

For reliable cancer imaging, Gd^{3+} ions are potential co-dopants to introduce magnetic properties, allowing for magnetic resonance imaging (MRI).[20] Aside from doping with Gd^{3+} ions, several groups investigated the suitability of Ln^{3+}-doped magnetic host materials as multimodal biomarkers that combine excellent optical and magnetic properties, allowing for high spatial resolution imaging via MRI. Here, gadolinium oxide, Gd_2O_3, is a promising host material.[21,22] Still, concerns may arise about leaching of free Gd^{3+} ions from the Gd_2O_3 nanophosphors causing toxicity. Yet, again, SiO_2[23] or PEG-based[24–26] (PEG, polyethylene glycol) surface modifications were shown to not only prevent aggregation, enhance blood retention, facilitate cellular uptake, and provide binding sites for targeting, but also prevent leaching and reduce cytotoxicity. Soga et al. evaluated the cytotoxic effects of PEG-*b*-PAAc (poly(ethylene glycol)-*b*-poly(acrylic acid) block co-polymer) -modified upconverting and NIR-emitting $Gd_2O_3:Er^{3+},Yb^{3+}$ nanostructures, and in contrast to unmodified nanostructures, no toxic effect was observed (Figure 3b).[27] Moreover, the NIR emission of 1.5 μm under 980 nm excitation is suitable for *in vivo* bioimaging, allowing for the observation of the biodistribution of such nanostructures in live mice (Figure 3c).

As previously mentioned, besides surface modification and dosage, particle size and morphology play a crucial role when it comes to risk assessment. In this context, *in vivo* MRI indicated the clearance of sub-10 nm lanthanide oxide particles through kidneys in mice, which is a prerequisite for clinical applications.[28] In contrast, larger nanoparticles and nanorods had been reported to accumulate in the liver, which may induce death of the mouse. Generally speaking, the toxicity of the nanostructures does not necessarily increase with increasing size. As observed by Venkatachalam et al.,[14] a decrease in the size of $Y_2O_3:Er^{3+}$ particles induced increasing toxicity toward macrophages. A size-comparison study by Lee et al. revealed a similar effect.[29] Consequently, careful risk assessment is required for different probes under different conditions. Heng et al. in their study emphasize the importance of rethinking commonly used laboratory protocols for cytotoxic assessment of nanomaterials.[30] The authors stress that, in particular, for mildly toxic nanomaterials, a longer duration cellular exposure is required for cytotoxic effects to become apparent, and most studies would not further investigate the post-exposure cell biology and physiology. This means not monitoring the cellular conditions after the nanoparticle exposure and subsequent reseeding of the cells onto new, nanoparticle-free culture plates.

It should be further mentioned that the interaction between biological matter and upconverting or NIR-emitting oxide nanostructures can be translated to other Ln^{3+} dopants or other Ln^{3+}-based host materials not showing upconversion or NIR emission. For example, Eu^{3+} or Tb^{3+}-doped Gd_2O_3 and Y_2O_3 emitting in the visible range under UV excitation were reported as non-toxic fluorescent labels.[15,31–33] Interestingly, cytotoxicity studies by Setua et al. revealed no reduction in the viability of normal and cancer cells when incubated with Y_2O_3 nanoparticles, nor was the formation of reactive oxygen species (ROS) observed; ROS are known to induce cell damage.[20]

https://doi.org/10.1557/mrs.2014.223 Published online by Cambridge University Press

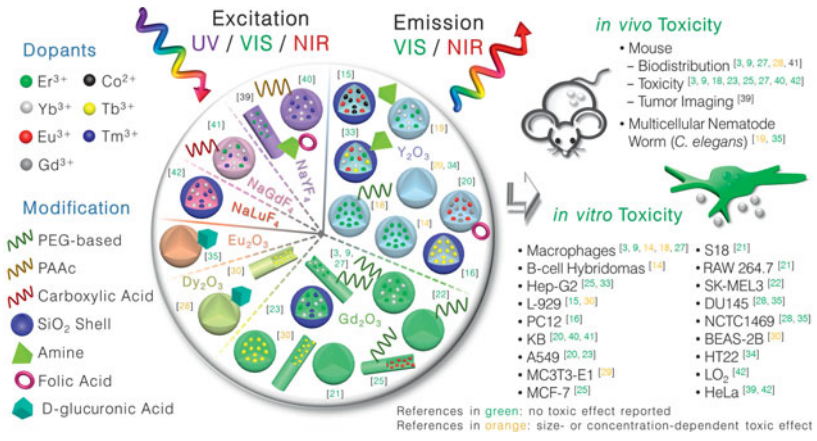
In fact, antioxidative properties that promote cell survival under conditions of oxidative stress have been reported for Y_2O_3.[34] Y_2O_3 and Gd_2O_3 may be the most intensively investigated oxide host materials for Ln^{3+}-doped nanophosphors, yet toxicity studies analyzing other lanthanide oxides, such as Eu_2O_3 and Dy_2O_3, indicate a similar non-toxic behavior, and they have been reported as promising candidates for bioimaging.[28,35]

Beyond oxides: Lanthanide-based fluorides

Biomedical applications often require ultra-small nanoparticles of 10 nm or less in size in order to avoid blockage of blood vessels, to allow cellular uptake, and to ensure clearance from the body. However, one must consider that oxide nanoparticles of such small sizes may suffer from quenching of their photoluminescence.[3] Yet, efficient emission in this size range is possible when Ln^{3+} ions are doped into a fluoride host matrix,[36–38] and upconverting non-toxic $NaYF_4$:Ln^{3+} nanoparticles have successfully been applied for *in vitro* cellular and *in vivo* animal imaging.[39,40] Investigations of the *in vivo* biodistribution revealed rather slow clearance from the body. However, long-term studies indicated that mice survive the injection for at least 115 days without any evident toxic effect. Further, $NaGdF_4$ has been suggested as a non-toxic host material for lanthanide doping that provides NIR-to-NIR upconversion luminescence in combination with magnetic properties.[41] Aiming for the fusion of information from several imaging techniques, GdDTPA (chelated gadolinium, diethylenetriamine pentaacetic acid)-complexed $NaLuF_4$: Tm^{3+}, Yb^{3+} nanoparticles were presented as a trimodal marker for NIR-to-NIR imaging, x-ray computed tomography, and MRI, enabling optical, x-ray-based, and magnetic imaging with one single marker. Again, the presented nanophosphors showed low cytotoxicity as indicated by *in vitro*, *in vivo*, and *ex vivo* studies.[42]

Summary: Challenges and perspectives

Significant progress has been made in the development of new Ln^{3+}-based nanoparticles as bioimaging probes. In addition to a broad range of requirements that must be fulfilled, including excellent optical properties, chemical and dispersion stability, and ideally multifunctionality, biocompatibility is the most crucial issue that has to be guaranteed prior to clinical applications. Here, a broad set of material properties and parameters such as concentration, morphology, size, surface charge, chemistry, and thermal and chemical stability need to be considered for comprehensive cytotoxic characterization. Moreover, there is the need to not only consider short-term, but also long-term toxicological effects that may be induced from potential biomarkers. The most recent efforts that have been undertaken by research groups around the globe reveal very promising results showing good biocompatibility of Ln^{3+}-doped oxide and fluoride nanostructures in combination with excellent optical properties (**Scheme 1**). This recent trend indicates that near-infrared emitting and upconverting lanthanide-based nanostructures indeed show promise for future optical bioimaging, yet the careful assessment of their (potentially long-term) toxicity remains a challenge that has to be addressed by materials scientists, biologists, and medical scientists.



Scheme 1. Overview of recent toxicity studies of lanthanide-based nanophosphors. Note: Macrophages, type of white blood cell; B-cell hybridomas, fused hybrid cells between B-cells (type of lymphocyte) and myeloma tumor cells; Hep-G2, human hepatocellular carcinoma cells; L-929, mouse fibroblastic cells; PC12, mouse melanoma cells; KB, human nasopharyngeal carcinoma cells; A549, human lung cancer cells; MC3T3-E1, mouse osteoblast-like cells; MCF-7, human breast adenocarcinoma cells; S18, human nasopharyngeal carcinoma cells; RAW264.7, murine macrophage line; SK-MEL3, human malignant melanoma cell line derived from lymph node; DU145, human prostate cancer cells; NCTC1469, normal mouse hepatocyte cells; BEAS-2B, human bronchial epithelial cells; HT22, mouse nerve cells; LO_2, normal human liver cells; HeLa, human cervical carcinoma cell line; PEG, poly(ethylene glycol); PAAc, poly(acrylic acid); UV, ultraviolet; VIS, visible; NIR, near-infrared.

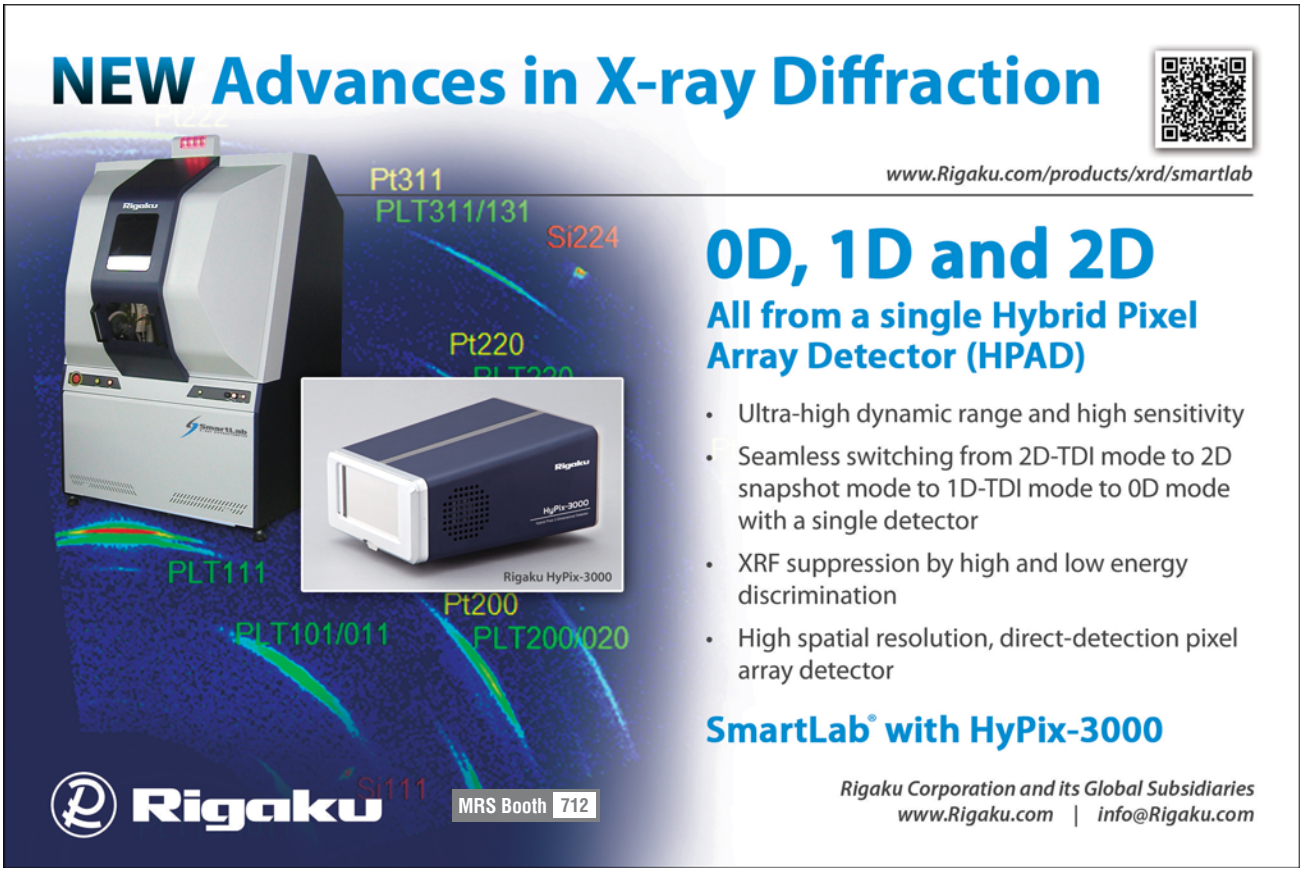
References

1. R.R. Anderson, J.A. Parrish, *J. Invest. Dermatol.* **77**, 13 (1981).
2. A.M. Smith, M.C. Mancini, S. Nie, *Nat. Nanotechnol.* **4**, 710 (2009).
3. E. Hemmer, N. Venkatachalam, H. Hyodo, A. Hattori, Y. Ebina, H. Kishimoto, K. Soga, *Nanoscale* **5**, 11339 (2013).
4. S.L. Troyan, V. Kianzad, S.L. Gibbs-Strauss, S. Gioux, A. Matsui, R. Oketokoun, L. Ngo, A. Khamene, F. Azar, J.V. Frangioni, *Ann. Surg. Oncol.* **16**, 2943 (2009).
5. C. Yao, Y. Tong, *Trends Analyt. Chem.* **39**, 60 (2012).
6. G. Blasse, B.C. Grabmaier, *Luminescent Materials* (Springer Verlag, Berlin, 1994).
7. K. Soga, in *Application of Ceramic Nanophosphors for Biomedical Photonics*, M.C. Tan, Ed. (Transworld Research Network, Kerala, India, 2009), p. 223.
8. F. Vetrone, J.A. Capobianco, *Int. J. Nanotechnol.* **5**, 1306 (2008).
9. E. Hemmer, H. Takeshita, T. Yamano, T. Fujiki, Y. Kohl, K. Löw, N. Venkatachalam, H. Hyodo, H. Kishimoto, K. Soga, *J. Mater. Sci. Mater. Med.* **23**, 2399 (2012).
10. Y. Mao, T. Tran, X. Guo, J.Y. Huang, C.K. Shih, K.L. Wang, J.P. Chang, *Adv. Funct. Mater.* **19**, 748 (2009).
11. T. Konishi, M. Shimizu, Y. Kameyama, K. Soga, *J. Mater. Sci. Mater. Electron.* **18** (S1), 183 (2007).
12. G.A. Sotiriou, M. Schneider, S.E. Pratsinis, *J. Phys. Chem. C* **115**, 1084 (2011).
13. M. Kamimura, N. Kanayama, K. Tokuzen, K. Soga, Y. Nagasaki, *Nanoscale* **3**, 3705 (2011).
14. N. Venkatachalam, E. Hemmer, T. Yamano, H. Hyodo, H. Kishimoto, K. Soga, *Prog. Cryst. Growth Charact. Mater.* **58**, 121 (2012).
15. T.Sh. Atabaev, O.S. Jin, J.H. Lee, D.-W. Han, H.H.T. Vu, Y.-H. Hwang, H.-K. Kim, *RSC Adv.* **2**, 9495 (2012).

https://doi.org/10.1557/mrs.2014.223 Published online by Cambridge University Press

16. G.A. Sotiriou, D. Franco, D. Poulikakos, A. Ferrari, *ACS Nano* **6**, 3888 (2012).
17. K. Soga, K. Tokuzen, K. Tsuji, T. Yamano, H. Hyodo, H. Kishimoto, *Eur. J. Inorg. Chem.* **18**, 2673 (2010).
18. N. Venkatachalam, T. Yamano, E. Hemmer, H. Hyodo, H. Kishimoto, K. Soga, *J. Am. Ceram. Soc.* **96**, 2759 (2013).
19. S.F. Lim, R. Riehn, C. Tung, W.S. Ryu, R. Zhuo, J. Dalland, R.H. Austin, *Nanotechnology* **20**, 405701 (2009).
20. S. Setua, D. Menon, A. Asok, S. Nair, M. Koyakutty, *Biomaterials* **31**, 714 (2010).
21. N. Luo, X. Tian, C. Yang, J. Xiao, W. Hu, D. Chen, L. Li, *Phys. Chem. Chem. Phys.* **15**, 12235 (2013).
22. G. Azizian, N. Riyahi-Alam, S. Haghgoo, M. Saffari, R. Zohdiaghdam, E. Gorj, *Mater. Sci. Poland* **31**, 158 (2013).
23. L. Zhou, Z. Gu, X. Liu, W. Yin, G. Tian, L. Yan, S. Jin, W. Ren, G. Xing, W. Li, X. Chang, Z. Hu, Y. Zhao, *J. Mater. Chem.* **22**, 966 (2012).
24. M. Ahrén, L. Selegard, A. Klasson, F. Söderlind, N. Abrikossova, C. Skoglund, T. Bengtsson, M. Engström, P.-O. Käll, K. Uvdal, *Langmuir* **26**, 5753 (2010).
25. Z. Liu, X. Liu, Q. Yuan, K. Dong, L. Jiang, Z. Li, J. Ren, X. Qu, *J. Mater. Chem.* **22**, 14982 (2012).
26. E. Hemmer, N. Venkatachalam, H. Hyodo, K. Soga, *Adv. Mater. Sci. Eng.* **2012**, 748098 (2012).
27. E. Hemmer, T. Yamano, H. Kishimoto, N. Venkatachalam, H. Hyodo, K. Soga, *Acta Biomater.* **9**, 4734 (2013).
28. K. Kattel, J.Y. Park, W. Xu, H.G. Kim, E.J. Lee, B.A. Bony, W.C. Heo, S. Jin, J.S. Baeck, Y. Chang, T.J. Kim, J.E. Bae, K.S. Chae, G.H. Lee, *Biomaterials* **33**, 3254 (2012).
29. S. Lee, T. Kasuga, K. Kato, *J. Ceram. Soc. Jpn.* **118**, 428 (2010).
30. B.C. Heng, G.K. Das, X. Zhao, L.-L. Ma, T.T.-Y. Tan, K.W. Ng, J.S.-C. Loo, *Biointerphases* **5**, FA88 (2010).
31. M. Nichkova, D. Dosev, S.J. Gee, B.D. Hammock, I.M. Kennedy, *Anal. Chem.* **77**, 6864 (2005).
32. R.M. Petoral Jr., F. Söderlind, A. Klasson, A. Suska, M.A. Fortin, N. Abrikossova, L. Selegård, P.-O. Käll, M. Engström, K. Uvda, *J. Phys. Chem. C* **113**, 6913 (2009).
33. G.K. Das, T.T.Y. Tan, *J. Phys. Chem. C* **112**, 11211 (2008).
34. D. Schubert, R. Dargusch, J. Raitano, S.-W. Chan, *Biochem. Biophys. Res. Commun.* **342**, 86 (2006).
35. K. Kattel, J.Y. Park, W. Xu, H.G. Kim, E.J. Lee, B.A. Bony, W.C. Heo, Y. Chang, T.J. Kim, J.Y. Do, K.S. Chae, Y.W. Kwak, G.H. Lee, *Colloids Surf. A* **394**, 85 (2012).
36. G. Chen, T.Y. Ohulchanskyy, R. Kumar, H. Agren, P.N. Prasad, *ACS Nano* **4**, 3163 (2010).
37. F. Vetrone, R. Naccache, A.J. de la Fuente, F. Sanz-Rodrıíguez, A. Blazquez-Castro, E. Martin Rodriguez, D. Jaque, J. García Solé, J.A. Capobianco, *Nanoscale* **2**, 495 (2010).
38. T. Cao, T. Yang, Y. Gao, Y. Yang, H. Hu, F. Li, *Inorg. Chem. Commun.* **13**, 392 (2010).
39. L.-Q. Xiong, Z.-G. Chen, M.-X. Yu, F.-Y. Li, C. Liu, C.-H. Huang, *Biomaterials* **30**, 5592 (2009).
40. L. Xiong, T. Yang, Y. Yang, C. Xu, F. Li, *Biomaterials* **31**, 7078 (2010).
41. J. Zhou, Y. Sun, X. Du, L. Xiong, H. Hua, F. Li, *Biomaterials* **31**, 3287 (2010).
42. A. Xia, M. Chen, Y. Gao, D. Wu, W. Feng, F. Li, *Biomaterials* **33**, 5394 (2012). □





https://doi.org/10.1557/mrs.2014.223 Published online by Cambridge University Press